Chapter 3

VISIBLE SUB-MICROMETER MICRODISK LASERS

3.1 Introduction

Semiconductor microdisk lasers based on micro-fabricated whispering gallery mode cavities have been studied for over 15 years, and were originally pioneered in InGaAsP material emitting in the near-infrared telecommunication wavelength range, as this material exhibits low surface recombination losses. High Q-factors, monolithic fabrication, and the possibility of dense integration make the microdisk geometry a very promising candidate for optical communications and chemical sensing. By selecting various material systems, microdisk lasers have been demonstrated at many different wavelengths ranging from the UV to the IR [1-6]. By depositing one contact on the top surface of the disk and establishing a conducting path from the laser through the substrate, electrical injection lasers have also been realized in this geometry [7-9]. Shrinking the disk size was shown to enable large-scale integration and low energy consumption. However, due to the high optical bend losses inherent to small disk microcavities, much research still focuses on cavity sizes over 2 μm in diameter. The smallest disk laser reported in the literature so far consisted of a 1.6 μm diameter "thumbtack" laser fabricated in the InGaAs/InGaAsP quantum well (QW) material system, emitting light at wavelength of 1.54 μm in 1993 [10].

In this chapter, we report even smaller visible microdisk lasers fabricated in InGaP/InGaAlP QW material and emitting light at a wavelength of approximately 645 nm.

The 645±5 nm diameter of our free-standing disk laser is about the same as the vacuum emission wavelength. To our knowledge the diameter relative to the wavelength is even smaller than previous reported results. Furthermore, the device operates at room temperature with a low excitation threshold of 50 μW. The cavity volumes of these laser devices, calculated to be approximately 0.03 μm^3, are well suited for the exploration of laser performance at the extreme limits of laser size. Ultra-small lasers in visible light emitting material systems are also expected to be excellent spectroscopy sources to perform very local chemical and biological measurements.

3.2 Ultra-small microdisk lasers

InGaP/InGaAlP quantum wells were grown by metal-organic chemical-vapor deposition (MOCVD) on top of a sacrificial AlGaAs layer, deposited onto a GaAs substrate. Optical gain was provided by two 7 nm thick and compressively strained InGaP quantum wells that were separated by 10 nm InGaAlP barriers (Figure 3.1 (a)). The active quaternary material was designed to emit light at ~670 nm (Figure 3.1 (b)). Due to the compressively strained quantum wells, light was strongly coupled into transverse electric (TE) modes. The quantum well active material was placed within the center of a 170 nm InGaAlP slab, and 10 nm InGaP lattice matched layers were used on the top and bottom sides of the slab to prevent the oxidation of aluminum in the quaternary compound. A 700 nm thick sacrificial AlGaAs layer was introduced between the slab and the GaAs substrate, designed to be removed through a selective chemical etch to avoid coupling losses from the disk wings into the substrate. Following epitaxial growth of the InGaP/InGaAlP material, the wafers were coated with a 100 nm

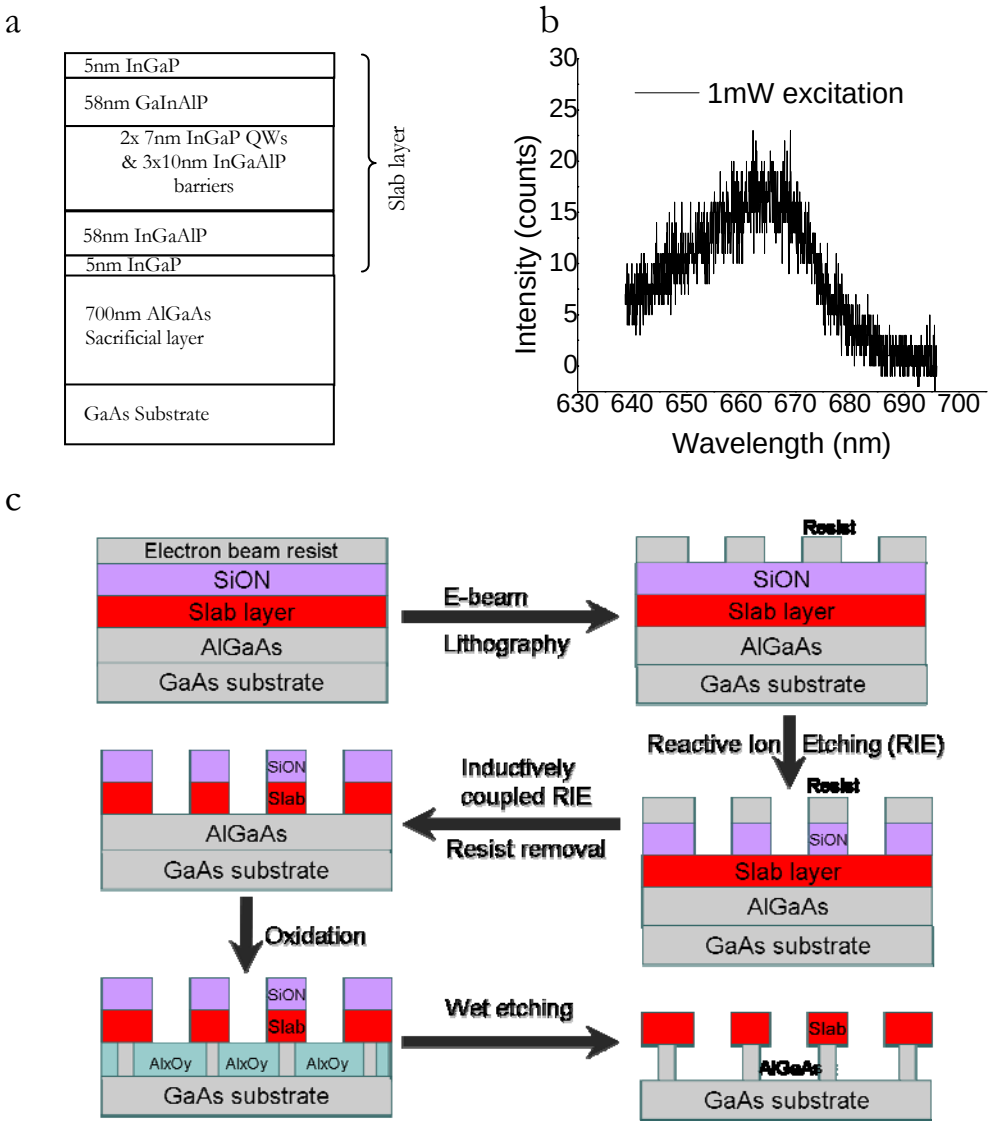

Figure 3.1 (a) Schematic epitaxial layer sequence of our slab composition and (b) a typical photoluminescence emission spectrum taken from the grown wafer. (c) The fabrication procedure flow chart

SiON hard mask and 200 nm ZEP520 electron beam resist.

Electron beam lithography was then used to define ring patterns within the ZEP520 electron beam resist (Figure 3.1c). The inner circles defined the disk diameters and the widths of the rings were designed to prevent optical coupling losses from the disk edge

into the surrounding quantum well material. Reactive ion etching (RIE) was subsequently used to directionally transfer the lithographic pattern from that resist into the SiON etch mask by using a CHF_3 plasma. After removal of the resist, the hard mask pattern was further transferred through the InGaP active layer with an iodine-based inductively coupled plasma reactive ion etch (ICP-RIE). Time-controlled steam oxidation of the AlGaAs by water vapor within a tube furnace followed by the potassium hydroxide (KOH) chemical dissolution of the resulting aluminum oxide formed the mushroom shaped microdisk structure shown in Figure 3.2. Dilute buffered HF was finally used to remove the SiON etch mask. As an alternative to electron beam lithography, it should also be possible to define the microdisk laser disks by photolithography, which provides the opportunity of high throughput production of ultra-small lasers. By defining a post radius to 0.2 μm smaller than that of the microdisk, we minimize the light leakage through the post while maintaining acceptable heat sinking of the active laser mode volume. We have fabricated and characterized many different sizes of disks, with diameters ranging from 1.6 μm down to 0.5 μm, by deliberately decreasing the diameter in 100 nm steps. In these laser arrays, we observe lasing in all of the disks except for the 0.5 μm diameter devices.

The microdisks were optically pumped at room temperature using 8 ns pulses separated by 30 μs periods (0.027% duty cycle) with a 408 nm InGaN semiconductor diode laser. The pump beam was focused onto the sample surface, vertically coupling the excitation light (Figure 3.2b) through a 50x objective lens to form a pump beam spot size less than 3 μm in diameter. Free space pumping does not require fine alignment of the optical fiber

to the disk, an advantage especially for the submicron disk sizes described here. Moreover, free space pumping covers the entire disk area and renders the cavity and the central part of the laser disk transparent to minimize re-absorption in the central disk portion. However, the pumping and collection of laser emission from the disk is not very efficient. The excitation powers used in this chapter were determined by dividing the reading of the power meter at the sample (averaged laser pulse power) by the duty cycle. The emission from the lasers was then collected through the same objective lens and lasing spectra were taken with a liquid-nitrogen-cooled charge coupled device (CCD) (Princeton instruments, Spec10) detector filtered by a monochromator (Acton, SpectraPro). The monochromator entrance slit width was set to a width of 10 μm and a 1200 g/mm grating was used, resulting in a spectral resolution of approximately 0.1 nm. An additional flip-up mirror was used to guide the light into a CCD imaging system to view images of laser cavity modes within the microdisks as well as the excitation pump spot.

Figure 3.2a shows an angled view of a completely fabricated ultra-small microdisk, taken in a scanning electron microscope (SEM). The sidewall roughness of the disk is less than 20 nm and the non-vertical sidewall is due to the non-optimized dry etching recipe which could be further improved. Figure 3.2b illustrates the excitation and detection scheme used in this experiment, and it should be noted that this free space pump-collection measurement scheme is not efficient, since a large portion of the

a

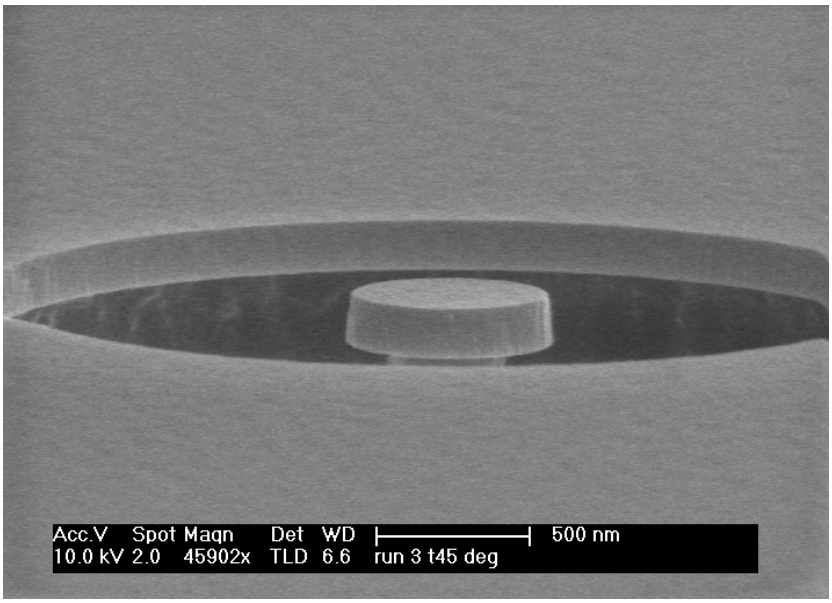

b

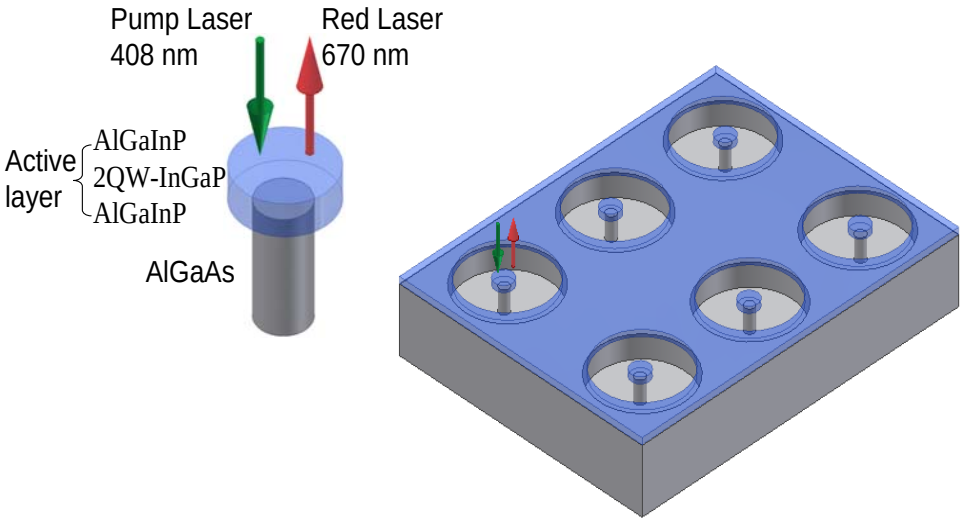

Figure 3.2. (a) Scanning electron microscope image of a 0.6 μm diameter submicron microdisk laser structure. (b) Illustration of mushroom shape structure and pumping scheme

excitation light does not couple into the mode. Indeed, much of the emitted light also escapes horizontally along the disk plane and vertically into the GaAs substrate. We

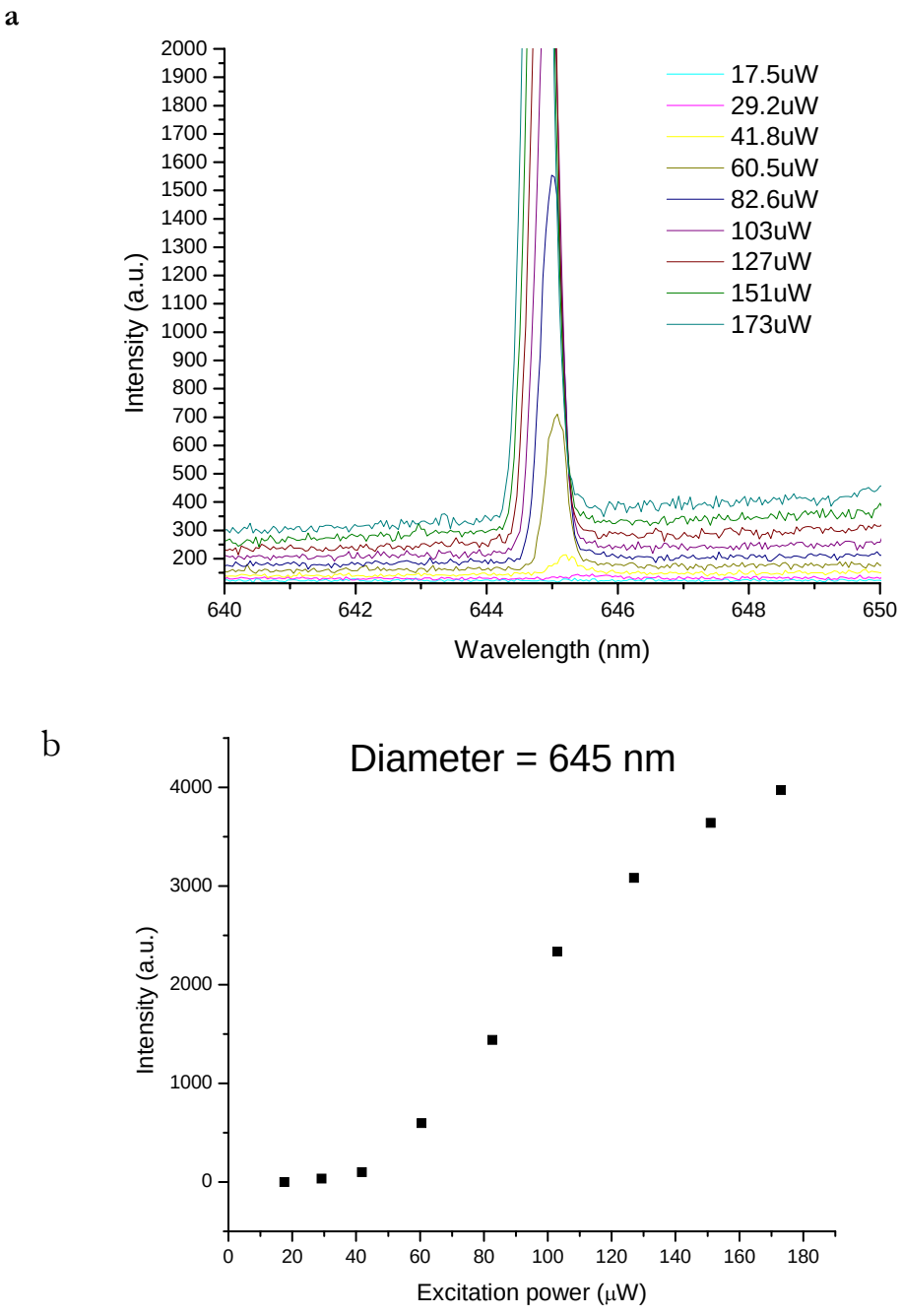

Figure 3.3. (a) The Spectra with different excitation power and (b) L-L curve of one of the 645 nm diameter microdisks

expect that much higher output power and lower thresholds can be observed when using fiber-coupling measurements. Figure 3.3 shows luminescence spectra and an L

(excitation power)-L (lasing peak intensity) curve from a device with disk diameter of 645 nm and post diameter of 200 nm. The laser threshold was measured to be approximately 50 μW. This threshold power is similar to that of photonic crystal slab lasers that we recently fabricated within the same InGaP material system [11]. The linewidth was measured as 0.4 nm at threshold, yielding an effective Q of about 1600. Above 120 μW, heating of the laser cavity ultimately limits the output power, and the L-L curve saturates. Figure 3.4 shows the lasing characteristics of another ultra-small microdisk with disk diameter of 650 nm and post diameter of 350 nm. The laser threshold was measured to be approximately 187 μW and saturation occurred when the power exceeded 250 μW. Linewidth of 0.5 nm was measured at threshold, corresponding to an effective Q of approximately 1300. Both cavities exhibited distinct threshold behavior with linear L-L response of the output power above threshold and before saturation. Figure 3.4 also shows the semi-logarithmic plot of the L-L curve, confirming the lasing characteristics. The difference in threshold and saturation powers in the two smallest lasers may be due to the larger size post of the 650 nm disk. In both cases, we observed a blue shift of the emission as the excitation power increased. This is due to an increase of effective refractive index, which is approximately proportional to the increase in carrier density. The modes for these ultra-small disk lasers need to be further studied [12]. Figure 3.5a shows spectra of some other lasers. Single-mode operation was maintained until the disk diameter was increased to 1 μm. The small peak to the right of the main peak from 1 μm disk may be a result of propagation direction degeneracy, caused by nonsymmetrical or random roughness from the fabrication process.

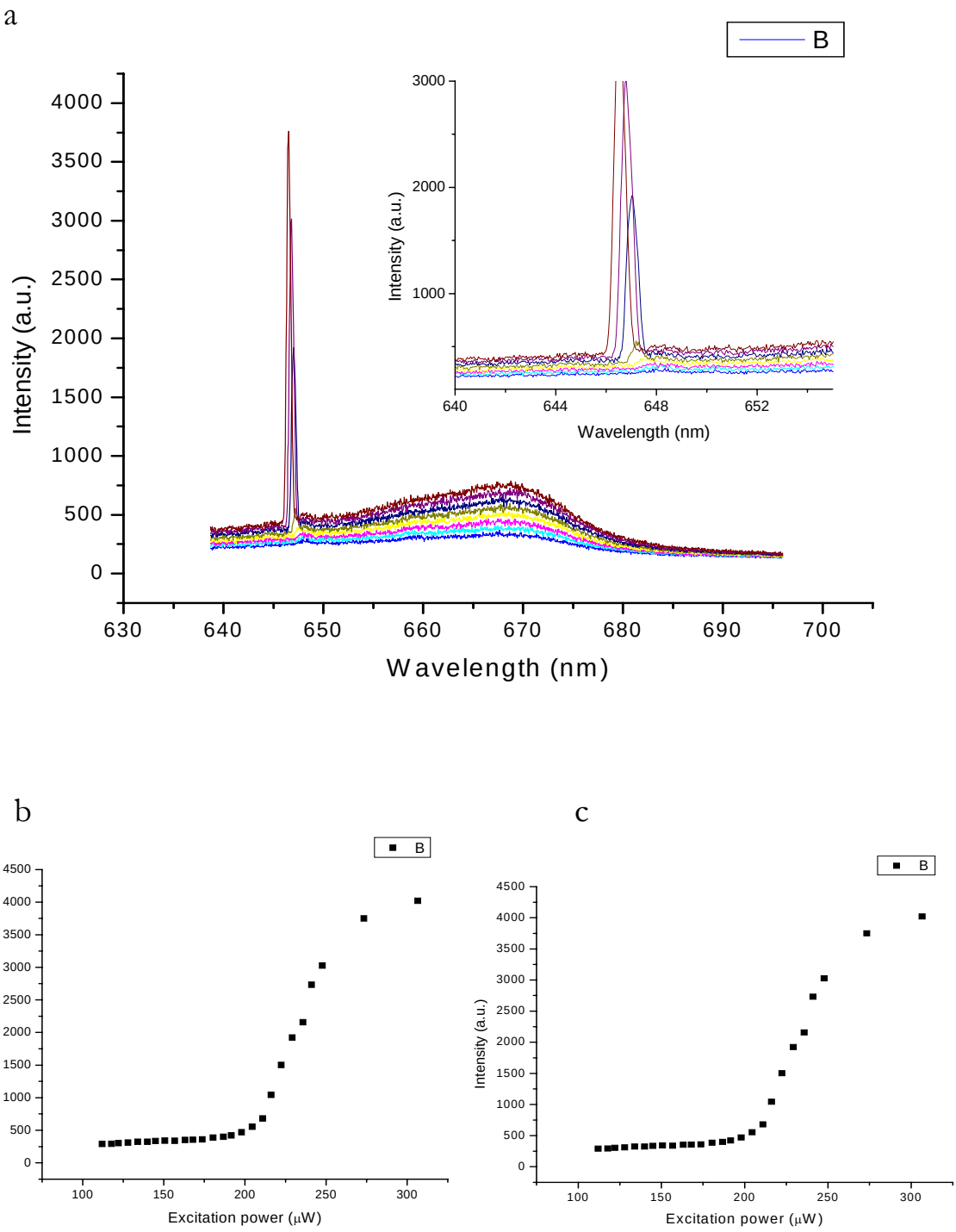

Figure 3.4. (a) The Spectra with different excitation powers and (b)(c) linear and semi-logarithmic plot of L-L curve of a 650 nm diameter microdisk

a

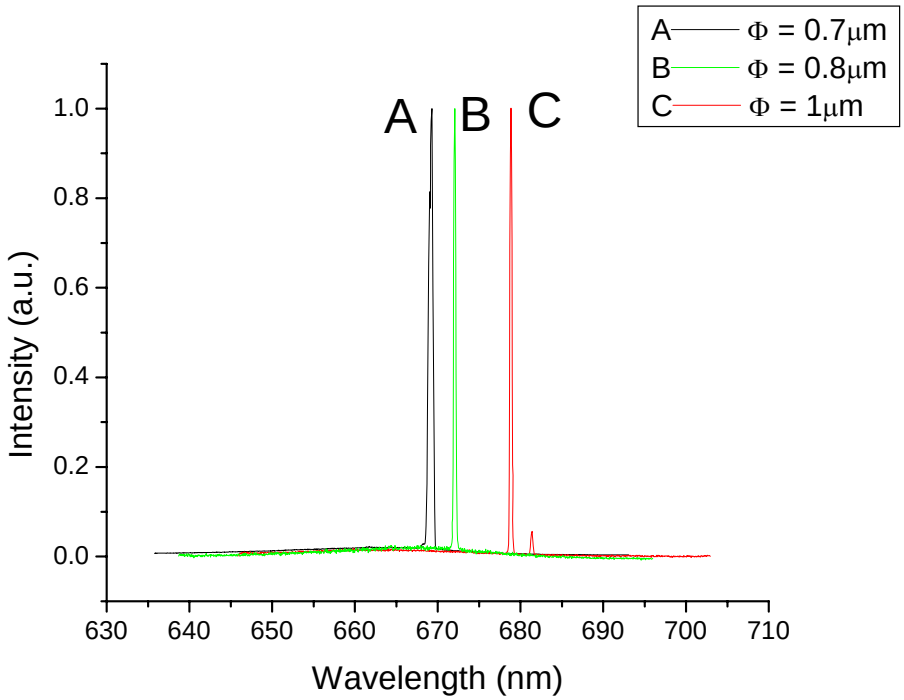

b

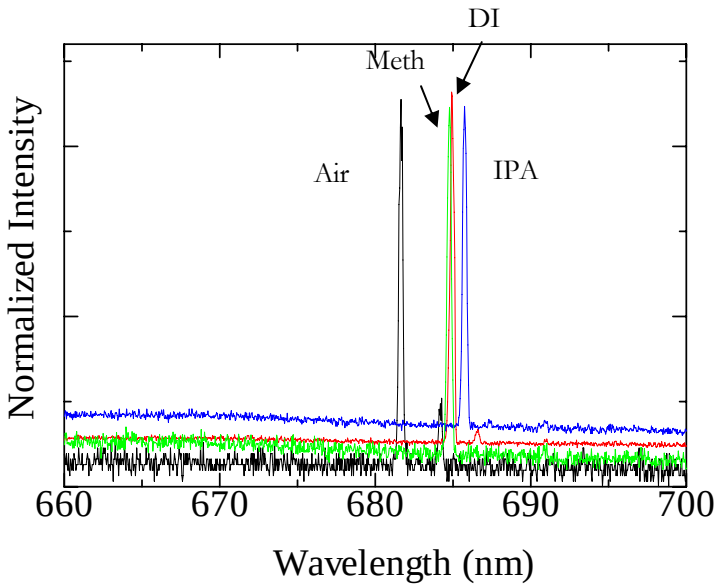

Figure 3.5. (a) Laser spectra with different diameter microdisks and (b) lasing peak wavelength shift obtained with different chemical environments. Black line denotes spectrum in air, green denotes spectrum in methanol, red denotes spectrum in DI water, and blue denotes the spectrum in IPA.

3.3 Microdisk lasers for refractive index monitoring

The use of microdisk lasers for spectroscopic analysis has been described earlier [13]. Here we use the ultra-small mode volume microdisk lasers to check the sensitivity to the environmental refractive index changes and molecules attached onto the disk surface. Figure 3.5b shows the spectra of a 1 μm diameter disk when used as a refractive index monitor. The lasing peak shifts from 681.6 nm to 684.8 nm when the disk is surrounded by methanol, to 684.9 nm in deionized water, and to 685.8 nm when immersed in isopropyl alcohol (IPA). The sensitivity of the microdisk is ~ 11 nm per refractive index unit (REU). We expect higher sensitivities in even smaller disks since the optical mode is more extended to the outside of the disk, and mode hopping can be avoided by utilizing disks that support only few modes. Compared to the results of optimized photonic crystal slab lasers, which provide a sensitivity of 179 nm per REU [14], the sensitivity of our disk laser is one magnitude lower, due to the difference in wavelength as well as the less optimal overlap between the lasing mode and the analyte to be measured. The ease of fabrication, along with the improved tolerance to dimensional imprecision and analyte refractive index, provides the disk structure with important advantages for local refractive index monitoring for chemical and biological analyses.

3.4 Conclusion

In this chapter, we have fabricated ultra-small disk lasers with optical mode volumes of only 0.03 μm^3 in InGaP QW material. We have demonstrated excitation thresholds as low as 50 μW in 645 nm disks at room temperature. We also show the lasing spectra from submicron microdisks with different diameters and explore the use of these ultra-small disk lasers for refractive index monitoring. We expect these InGaP red sub-micron microdisk

lasers to be very useful for biochemical analysis as well as for efficient light emitters in the near future.

Bibliography

1. Mccall, S.L., et al., *Whispering-Gallery Mode Microdisk Lasers.* Applied Physics Letters, 1992. **60**(3): 289-291.
2. Mohideen, U., et al., *Gaas/Algaas Microdisk Lasers.* Applied Physics Letters, 1994. **64**(15): 1911-1913.
3. Pan, J.S., et al., *0.66 mu m InGaP/InGaAlP single quantum well microdisk lasers.* Japanese Journal of Applied Physics Part 2-Letters, 1998. **37**(6A): L643-L645.
4. Hovinen, M., et al., *Blue-Green Laser-Emission from Znse Quantum-Well Microresonators.* Applied Physics Letters, 1993. **63**(23): 3128-3130.
5. Chang, S.S., et al., *Stimulated emission and lasing in whispering-gallery modes of GaN microdisk cavities.* Applied Physics Letters, 1999. **75**(2): 166-168.
6. Michler, P., et al., *A quantum dot single-photon turnstile device.* Science, 2000. **290**(5500): 2282-.
7. Levi, A.F.J., et al., *Room-Temperature Operation of Microdisk Lasers with Submilliamp Threshold Current.* Electronics Letters, 1992. **28**(11): 1010-1012.
8. Baba, T., et al., *Lasing characteristics of GaInAsP-InP strained quantum-well microdisk injection lasers with diameter of 2-10 mu m.* IEEE Photonics Technology Letters, 1997. **9**(7): 878-880.
9. Zhang, L.D. and E. Hu, *Lasing emission of InGaAs quantum dot microdisk diodes.* IEEE Photonics Technology Letters, 2004. **16**(1): 6-8.
10. Levi, A.F.J., et al., *Room-Temperature Operation of Submicrometer Radius Disk Laser.* Electronics Letters, 1993. **29**(18): 1666-1668.

11. Zhang, Z., et al., *Visible two-dimensional photonic crystal slab laser.* Applied Physics Letters, 2006. **89**(7).

12. Gmachl, C., et al., *High-power directional emission from microlasers with chaotic resonators.* Science, 1998. **280**(5369): 1556-1564.

13. Fang, W., et al., *Detection of chemical species using ultraviolet microdisk lasers.* Applied Physics Letters, 2004. **85**(17): 3666-3668.

14. Loncar, M., A. Scherer, and Y.M. Qiu, *Photonic crystal laser sources for chemical detection.* Applied Physics Letters, 2003. **82**(26): 4648-4650.